# Influence of Acoustic Phonons on Tunneling through Metal-Oxide-Semiconduction Junctions*

H. J. DEULING
*Department of Physics and Materials Research Laboratory, University of Illinois, Urbana, Illinois 61801*
(Received 18 July 1969)

The electronic proper self-energy due to electron–acoustic-phonon interaction in degenerate semiconductors has been evaluated with second-order perturbation theory. This self-energy has been used to calculate the conductance and $d^2I/dV^2$ of metal-oxide-semiconductor tunnel junctions. A simple uniform-field model for the barrier-penetration factor has been used in this calculation. The predicted line shapes show a sharp structure at $eV=2\hbar c_s k_F$, which is washed out as the impurity scattering lifetime is decreased. In contrast to analogous calculations for interaction with optical phonons, the predicted structure is due to the dependence of the self-energy on momentum rather than on energy.

WITHIN the framework of the transfer-Hamiltonian model[1–3] of electron tunneling there exist two mechanisms by which collective excitations can influence the tunneling. One of these is inelastic tunneling where an electron excites a collective mode "while" it tunnels. The second mechanism consists of interaction of the tunneling electron with collective modes in the electrodes and is known as self-energy effect. This effect has been studied extensively for interaction of the electrons with optical phonons[4–6] and with plasmons.[7] A self-energy effect due to deformation-potential coupling between electrons and acoustic phonons is investigated in this paper.

If a free-electron model is used for the metal electrode of the tunnel junction and if the barrier penetration factor is assumed to be independent of the bias voltage, the tunnel conductance $dI/dV$ at $T=0$ is given by[3–5]

$$\frac{dI}{dV}=\frac{2e^2A}{\pi h}\int_{-\zeta}^{\infty}d\xi_{\mathbf{k}}\,\mathrm{Im}G(\xi_{\mathbf{k}},-eV)\times\int\frac{d^2\mathbf{k}_{\parallel}}{(2\pi)^2}D(\mathbf{k}_{\parallel},\xi_{\mathbf{k}}),\quad(1)$$

where

$$\xi_{\mathbf{k}}=\hbar^2\mathbf{k}^2/2m^*-\zeta.\quad(2)$$

$\zeta$ is the Fermi level, $A$ is the surface area of the junction, $D(\mathbf{k}_{\parallel},\xi_{\mathbf{k}})$ is the barrier penetration factor, and $G(\xi_{\mathbf{k}},\epsilon)$ is the Green's function in the semiconductor electrode.

For the uniform-field model[3] of a metal-semiconductor contact, the barrier penetration factor is

$$D=D_0\exp(-\hbar^2\mathbf{k}_{\parallel}^2/2m^*E_0).\quad(3)$$

The constants $D_0$ and $E_0$ can be determined by fitting the background conductance. The integral over $\mathbf{k}_{\parallel}$ in Eq. (1) can now easily be carried out and $dI/dV$ is given by

$$\frac{dI}{dV}=\frac{4e^2m^*AD_0E_0}{h^2}\int_{-\zeta}^{\infty}d\xi_{\mathbf{k}}\,\mathrm{Im}G(\xi_{\mathbf{k}},-eV)\times\{1-\exp[-(\xi_{\mathbf{k}}+\zeta)/E_0]\}.$$

The Green's function $G(\xi_{\mathbf{k}},\epsilon)$ can be expressed in terms of $\xi_{\mathbf{k}}$, energy $\epsilon$ and the proper electronic self-energy $\Sigma(\xi_{\mathbf{k}},\epsilon)$. The self-energy $\Sigma(\xi_{\mathbf{k}},\epsilon)$ has been calculated with the lowest-order diagram [Fig. 4(a)] by perturbation theory. To include the scattering of electrons by impurities, the free-electron line in the diagram has been renormalized with a finite lifetime, i.e., instead of the free-electron propagator, the renormalized Green's function

$$G=1/(\epsilon-\xi_{\mathbf{k}}+i\Gamma)$$

has been used to calculate the self-energy. $\hbar/2\Gamma$ is the impurity scattering lifetime. Figure 1 shows the real and imaginary parts of the self-energy as a function of energy for $k=k_F$ and $\Gamma=0$. The mass renormalization is very small, $\mathrm{Im}\Sigma$ shows a sharp drop at $E=\pm2\hbar c_s k_F$. Near $E=0$ $\mathrm{Im}\Sigma$ varies as $|E|^3$. When $\Gamma$ is increased, the sharp edges in $\mathrm{Im}\Sigma$ are rounded off, as is seen in Fig. 2.

The tunnel conductance $dI/dV$ was found by doing the integral over $\xi_{\mathbf{k}}$ numerically on the IBM 360/75 computer at the University of Illinois. The $\mathbf{k}$ dependence of $\mathrm{Re}\Sigma(\xi_{\mathbf{k}},\epsilon)$ causes an antisymmetric structure in $dI/dV$: a small peak in reverse bias and a dip in forward bias. The imaginary part of $\Sigma(\xi_{\mathbf{k}},\epsilon)$ causes a symmetrical structure in $dI/dV$; a dip in forward and reverse bias. The two effects just cancel in reverse bias and add up in forward bias to give a dip in $dI/dV$ at $eV=2\hbar c_s k_F$ ($c_j$ is the velocity of sound, $k_F$ is the Fermi momentum). The dip in the conductance is fairly sharp for small $\Gamma$ but is rounded off and broadened

* Work supported in part by the Advanced Research Projects Agency under Contract No. SD-131.

[1] J. Bardeen, Phys. Rev. Letters 6, 57 (1961).
[2] M. H. Cohen, L. M. Falicov, and J. C. Phillips, Phys. Rev. Letters 8, 316 (1962).
[3] C. B. Duke, *Tunneling in Solids* (Academic Press Inc., New York, 1969).
[4] L. C. Davis and C. B. Duke, Solid State Commun. 6, 193 (1968).
[5] L. C. Davis and C. B. Duke, Phys. Rev. (to be published).
[6] F. Steinrisser, L. C. Davis, and C. B. Duke, Phys. Rev. 176, 912 (1968).
[7] C. B. Duke, M. J. Rice, and F. Steinrisser, Phys. Rev. (to be published).
[8] A. A. Abrikosov, L. P. Gorkov, and I. E. Dzyaloshinski, *Methods of Quantum Field Theory in Statistical Physics* (Pergamon Press, Inc., New York, 1965) Chaps. II, IV.

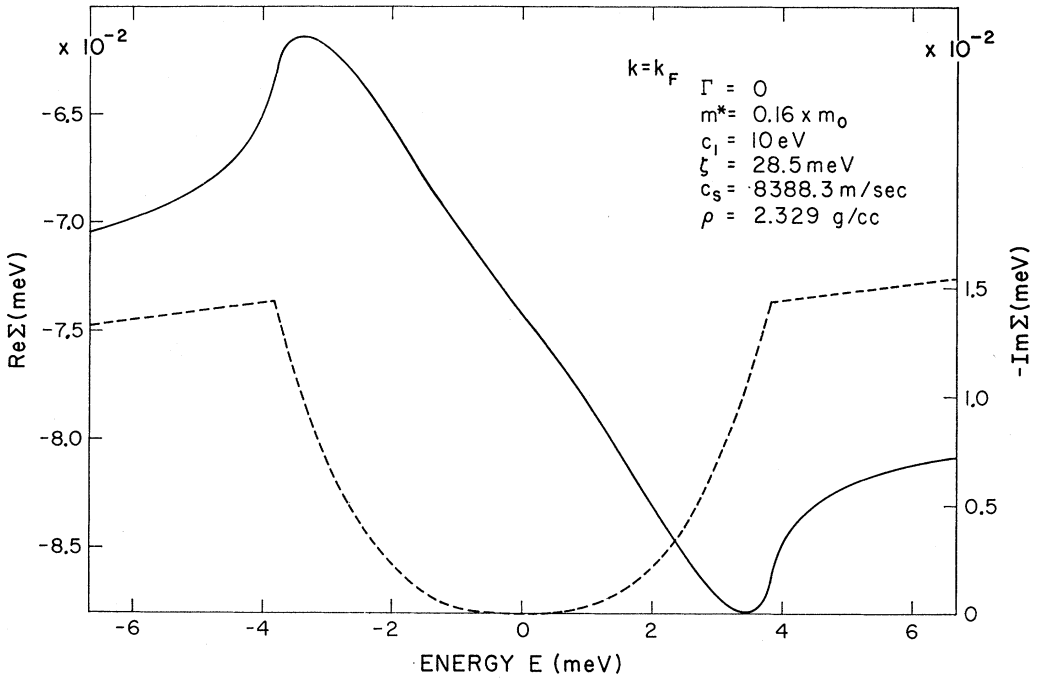


FIG. 1. Real part (solid line) and imaginary part (dashed line) of the proper electronic self-energy as a function of energy $\epsilon$ at fixed momentum $k=k_F$ and $\Gamma=0$.

if $\Gamma$ is increased. The second derivative $d^2I/dV^2$ was obtained by numerical differentiation. Figure 3 shows curves $d^2I/dV^2$ versus bias voltage for three different values of $\Gamma$ for $p$-type silicon. The curves show a sharp structure at $eV=2\hbar c_s k_F$ for small $\Gamma$. As $\Gamma$ is increased by two orders of magnitude, the structure is almost wiped out.

The conclusion from this calculation is that there is

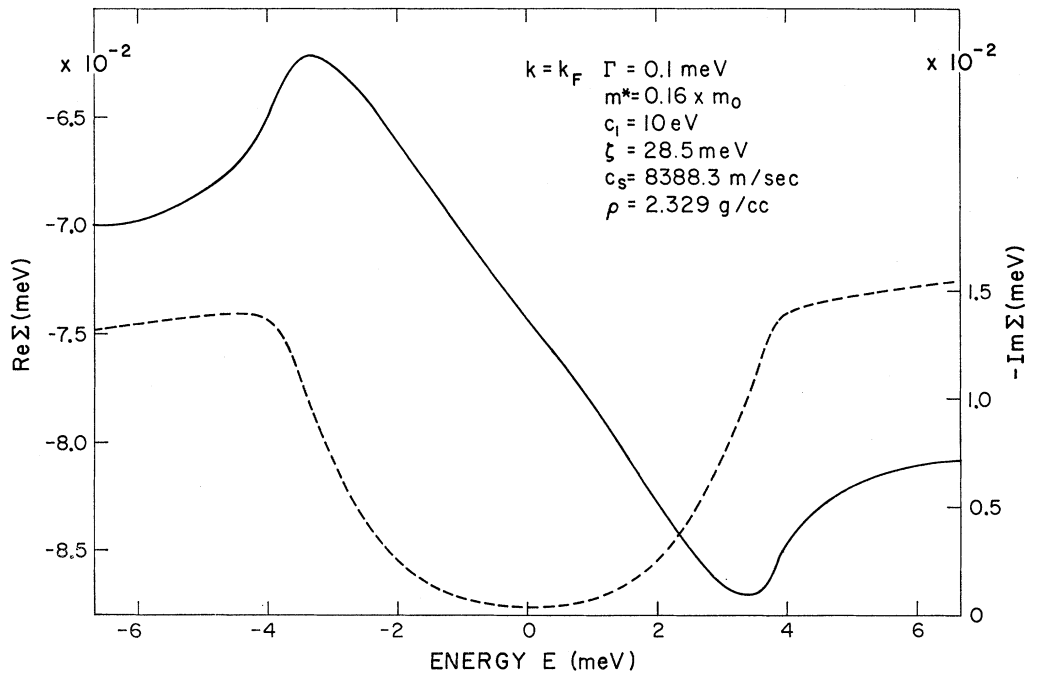


FIG. 2. Real part (solid line) and imaginary part (dashed line) of the self-energy as a function of energy at $k=k_F$ and $\Gamma=0.1$ MeV.

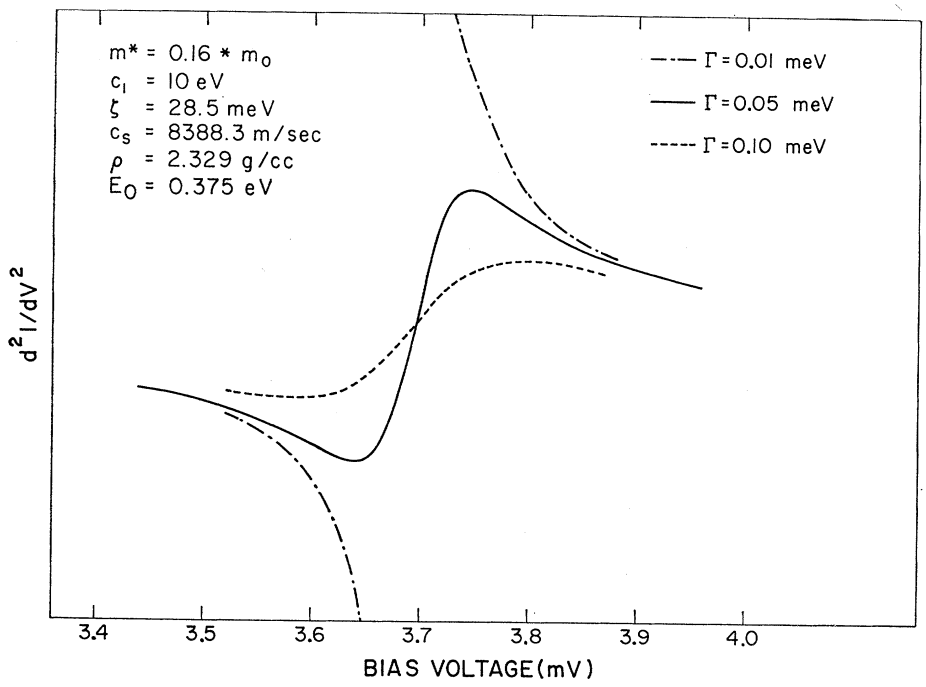


FIG. 3. $d^2I/dV^2$ versus bias voltage $V$ for three different values of $\Gamma$. For small $\Gamma$, the dip in $dI/dV$ at $eV=2\hbar c_s k_F$ has a sharp point resulting in a discontinuity in $d^2I/dV^2$. As $\Gamma$ is increased, the dip in $dI/dV$ is rounded off and giving a smooth curve for $d^2I/dV^2$.

a small self-energy effect due to acoustic phonons at bias voltage $eV=2\hbar c_j k_F$. The effect decreases with decreasing impurity scattering lifetime.

The author is indebted to Dr. L. C. Davis and Dr. C. B. Duke for very helpful discussions on this problem.

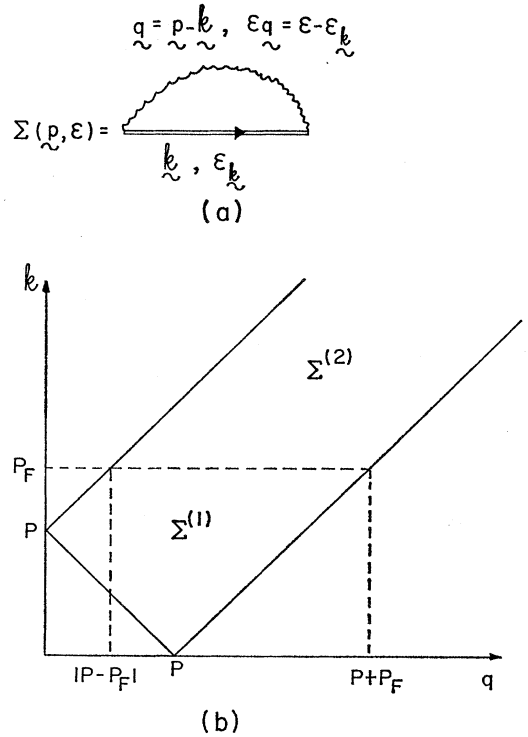


FIG. 4. (a) Diagram for the evaluation of $\Sigma$. (b) Area of integration in the $k$-$q$ plane for $\Sigma^{(1)}$ and $\Sigma^{(2)}$.

## APPENDIX: EVALUATION OF ELECTRONIC SELF-ENERGY

The electronic self-energy due to deformation-potential interaction of electrons with acoustic phonons is calculated with the lowest-order diagram [Fig. 4(a)]. The wavy line corresponds to the free phonon propagator.

$$D^0(\mathbf{q},\epsilon_q)=2\hbar\omega_q/[\epsilon_q^2-(\hbar\omega_q)^2],$$

where $\omega_q=c_s\cdot|\mathbf{q}|$ for acoustic phonons ($c_s$ is the velocity of sound). The solid line corresponds to the electron Green's function

$$G(\mathbf{k},\epsilon_k)=\left(\epsilon_k+\zeta-\frac{\hbar^2}{2m^*}\mathbf{k}^2+i\Gamma\right)^{-1},$$

which describes free electrons with impurity scattering in a phenomenological way. The matrix element for the interaction is

$$V_q=c_1^2\hbar c_s|\mathbf{q}|/2\rho c_s^2,$$

where $c_1$ is the coupling constant, $\rho$ is the density, and $c_s$ is the velocity of sound. The self-energy at $T=0$ is then given by

$$\Sigma=\Sigma^{(1)}+\Sigma^{(2)},$$

$$\Sigma^{(1)}(p,E)=\frac{c_1^2\hbar}{2\rho c_s(2\pi)^2 p}\times\int\int\frac{q^2\,dq k\,dk}{E+\zeta-(\hbar^2k^2/2m^*)+\hbar c_s q+i\Gamma},$$

$$\Sigma^{(2)}(p,E)=\frac{c_1^2\hbar}{2\rho c_s(2\pi)^2 p}\times\int\int\frac{q^2\,dq\,dk}{E+\zeta-(\hbar^2k^2/2m^*)-\hbar c_s q+i\Gamma}.$$

The area of integration in the $k$-$q$ plane is shown in Fig. 4(b) for $\Sigma^{(1)}$ and $\Sigma^{(2)}$. If the $k$ integral is performed first, the remaining $q$ integral can be divided into three intervals according to Fig. 4(b):

(i) $0\leq q\leq|p-p_F|$. In this region there is a contribution to $\Sigma^{(1)}$ only if $p<p_F$ and to $\Sigma^{(2)}$ only if $p>p_F$.

(ii) $|p-p_F|\leq q\leq p+p_F$. In this interval there is a contribution to $\Sigma^{(1)}$ and to $\Sigma^{(2)}$.

(iii) $p+p_F<q$. In this region there is a contribution to $\Sigma^{(2)}$ only.

The $k$ integral is easily performed. In the $q$ integral we substitute $x=\hbar q/(2m^*)^{1/2}$ and integrate up to a cutoff momentum $q_c$. The final result is found to vary very little with $q_c$. We introduce further the following notation:

$$\xi_p=\hbar^2p^2/2m^*-\zeta,\quad \eta=\tfrac{1}{2}m^*c_s^2,$$
$$x_1=\min\{\hbar q_c/(2m^*)^{1/2},\ |(\zeta)^{1/2}(\xi_p+\zeta)^{1/2}|\},$$
$$x_2=\min\{\hbar q_c/(2m^*)^{1/2},\ (\zeta)^{1/2}+(\xi_p+\zeta)^{1/2}\},$$
$$y_1=(\eta)^{1/2}+(\xi_p+\zeta)^{1/2},\quad y_2=(\eta)^{1/2}-(\xi_p+\zeta)^{1/2},$$
$$z_1=E+\zeta+2[\eta\cdot(\xi_p+\zeta)]^{1/2},$$
$$z_2=E+\zeta-2[\eta\cdot(\xi_p+\zeta)]^{1/2},$$
$$f_1(x,y,z)=\frac{1}{2}\int^x x^2\ln\{[(x+y)^2-z]^2+\Gamma^2\}\,dx,$$
$$f_2(x,y)=\frac{1}{2}\int^x x^2\ln\{[2(\eta)^{1/2}\cdot x+y]^2+\Gamma^2\}\,dx,$$
$$g_1(x,y,z)=\int^x x^2\tan^{-1}\left(\frac{(x+y)^2-z}{\Gamma}\right)dx,$$
$$g_2(x,y)=\int^x x^2\tan^{-1}\left(\frac{2(\eta)^{1/2}x+Y}{\Gamma}\right)dx,$$
$$\theta(x)=0,\quad x\leq 0$$
$$=1,\quad x>0.$$

In this notation $\Sigma(\xi_p,E)$ is given by the following expression:

$$\mathrm{Re}\Sigma(\xi_p,E)=-\tfrac{1}{2}\pi C_1^2\frac{m^*}{\rho}\left[\frac{(2m^*c_s)^{1/2}}{h}\right]^3[\eta(\xi_p+\zeta)]^{-1/2}\Big\{\theta(-\xi_p)[f_1(x_1,-y_2,z_2)-f_1(0,-y_2,z_2)$$
$$-f_1(x_1,-y_1,z_1)+f_1(0,-y_1,z_1)]+\theta(\xi_p)[f_1(x_1,y_1,z_1)-f_1(0,y_1,z_1)-f_1(x_1,y_2,z_2)+f_1(0,y_2,z_2)]$$
$$+f_2(x_2,E)-f_2(x_1,E)-f_1(x_2,-y_1,z_1)+f_1(x_1,-y_1,z_1)-f_2(x_2,-E)+f_2(x_1,-E)$$
$$+f_1\left(\frac{\hbar q_c}{(2m^*)^{1/2}},y_1,z_1\right)-f_1(x_1,y_1,z_1)-f_1\left(\frac{\hbar q_c}{(2m^*)^{1/2}},y_2,z_2\right)+f_1(x_2,y_2,z_2)\Big\}.$$

$$\mathrm{Im}\Sigma(\xi_p,E)=-\tfrac{1}{2}\pi c_1^2\frac{m^*}{\rho}\left(\frac{(2m^*c_s)^{1/2}}{h}\right)^3[\eta(\xi_p+\zeta)]^{-1/2}\Big\{\theta(-\xi_p)[g_1(x_1,-y_2,z_2)-g_1(0,-y_2,z_2)$$
$$-g_1(x_1,-y_1,z_1)+g_1(0,-y_1,z_1)]+\theta(\xi_p)[g_1(x_1,y_1,z_1)-g_1(0,y_1,z_1)-g_1(x_1,y_2,z_2)+g_1(0,y_2,z_2)]$$
$$-g_2(x_2,E)+g_2(x_1,E)-g_1(x_2,-y_1,z_1)+g_1(x_1,-y_1,z_1)-g_2(x_2,-E)+g_2(x_1,-E)$$
$$+g_1\left(\frac{\hbar q_c}{(2m^*)^{1/2}},y_1,z_1\right)-g_1(x_1,y_1,z_1)-g_1\left(\frac{\hbar q_c}{(2m^*)^{1/2}},y_2,z_2\right)+g_1(x_2,y_2,z_2)\Big\}.$$

The integrals defining $g_2(x,y)$ and $f_2(x,y)$ can be found in any integral table. The more complicated integrals $f_1(x,y,z)$ and $g_1(x,y,z)$ are given below as follows:

$$f_1(x,y,z)=\{\tfrac{1}{6}(x+y)^3-\tfrac{1}{2}y(x^2+xy-z)\}\ln\{[(x+y)^2-z]^2+\Gamma^2\}-\Gamma y\tan^{-1}\frac{(x+y)^2-z}{\Gamma}$$
$$+(\tfrac{1}{3}\beta z+\tfrac{1}{3}\Gamma\alpha+y^2\beta)\left\{\tan^{-1}\frac{x+y-\alpha}{\beta}+\tan^{-1}\frac{x+y+\alpha}{\beta}\right\}+(\tfrac{1}{6}\beta\Gamma-\tfrac{1}{6}\alpha z-\tfrac{1}{2}\alpha y^2)$$
$$\times\ln\frac{(x+y-\alpha)^2+\beta^2}{(x+y+\alpha)^2+\beta^2}-\frac{2}{9}(x+y)^3-\tfrac{2}{3}z(x+y)+y(x^2-y^2-z),$$

$$g_1(x,y,z)=\tfrac{1}{3}(x^3+y^3)\tan^{-1}\frac{(x+y)^2-z}{\Gamma}+\tfrac{1}{2}\Gamma y\ln\{[(x+y)^2-z]^2+\Gamma^2\}+\tfrac{1}{3}[\Gamma\cdot\beta-\alpha(z+3y^2)]$$

$$\times\left\{\tan^{-1}\frac{x+y-\alpha}{\beta}+\tan^{-1}\frac{x+y+\alpha}{\beta}\right\}-\tfrac{1}{6}[\alpha\Gamma+\beta(z+3y^2)]\ln\frac{(x+y-\alpha)^2+\beta^2}{(x+y+\alpha)^2+\beta^2}-\tfrac{2}{3}\Gamma(x+y),$$

where

$$\alpha=\frac{1}{\sqrt{2}}[(z^2+\Gamma^2)^{1/2}+z]^{1/2},\quad \beta=\frac{1}{\sqrt{2}}[(z^2+\Gamma^2)^{1/2}-z]^{1/2}.$$

PHYSICAL REVIEW B VOLUME 1, NUMBER 4 15 FEBRUARY 1970

# Shapes of Two-Phonon Recombination Peaks in Silicon†

N. O. FOLLAND
*Kansas State University, Manhattan, Kansas 66502*

(Received 14 April 1969; revised manuscript received 17 October 1969)

The radiative recombination spectrum of excitons in *n*-type Si exhibits structure which has been analyzed in terms of one- and two-phonon processes. A model for radiative recombination of excitons is presented which predicts one-phonon peak shapes which are in good agreement with experiment and two-phonon peak shapes which are in fair agreement with experiment. Calculations are described with particular attention devoted to phonon decoupling approximations. The observed width of the $\Delta_1(25)$ two-phonon peak is accounted for very well by phonon dispersion effects. Neither the $\Sigma_1(60)$ nor the $\Gamma_{25'}(64)$ two-phonon peak alone can span the observed width of the assigned peak. We conclude that this peak is composite. The calculations provide the following best estimates of the magnitudes (meV) of intervalley electron-phonon matrix elements $\Delta_1(25)$-261, $\Sigma_1(48)$-80, $\Sigma_1(60)$-178, and the intravalley (valence band) matrix element $\Gamma_{25'}(64)$-403 where the phonons are designated by their symmetry and energy (meV). Also included are certain intermediate results which show the effects of the approximations and permit modifications of the model to be tested without extensive calculation.

## 1. INTRODUCTION

STRUCTURE observed in the intrinsic radiative recombination spectrum of excitons in *n*-type Si can be understood in terms of one- and two-phonon processes.[1] Reasonable assignments of the phonons involved can be made on the basis of the selection rules and the experimental phonon spectrum.[1,2] However, some ambiguities remain which cannot be resolved by such considerations alone.

In this paper is presented a model for the calculation of the shapes of radiative recombination peaks. It is the purpose of this paper to show that the largest two-phonon peak is composite and has major contributions involving a $\Sigma_1$ intervalley phonon and a $\Gamma_{25'}$ intravalley phonon. Detailed calculations are described of the shapes of the principal two-phonon recombination peaks from Si. The calculations are of theoretical interest in that they lead to the evaluation of the absolute magnitudes of those electron-phonon matrix elements which control transport processes.[3,4] In previous calculations of this type, only the integrated intensities were used to relate the experimental results to the electron-phonon coupling constants.[1,5] There was no basis to choose between equally tenable interpretations. Besides clarifying the interpretation of the two-phonon peaks the calculations reveal the effects of decoupling approximations.

The many-valley picture of the band structure of Si is briefly reviewed in Sec. 2 in the context of radiative recombination. The exciton radiative recombination intensity is expressed quantitatively in terms of matrix elements between one-electron Bloch states in Sec. 3. In Sec. 4, various levels of approximation and the results obtained are described and discussed. Calculated results are compared with experiment and empirical values obtained for the electron-phonon coupling constants in Sec. 5. Finally, in Sec. 6, the present results and conclusions are discussed in light of related work.

† Work supported in part by the Office of Naval Research under Themis Contract No. N00014-68-A-0504.

[1] W. P. Dumke, Phys. Rev. **118**, 938 (1960).

[2] P. J. Dean, J. R. Haynes, and W. F. Flood, Phys. Rev. **161**, 711 (1967).

[3] D. Long, Phys. Rev. **120**, 2024 (1960).

[4] J. E. Aubrey, W. Gubler, T. Henningsen, and S. H. Koenig, Phys. Rev. **130**, 1667 (1963).

[5] N. O. Folland, Phys. Letters **27A**, 708 (1968).